Resonance effects on the Raman spectra of graphene superlattices

V. Carozo,[1,2] C. M. Almeida,[1] B. Fragneaud,[1] P. M. Bedê,[1] M. V. O. Moutinho,[3] J. Ribeiro-Soares,[4] N. F. Andrade,[5] A. G. Souza Filho,[5] M. J. S. Matos,[4] B. Wang,[6] M. Terrones,[6] Rodrigo B. Capaz,[1,3] A. Jorio,[4] C. A. Achete,[1,2] and L. G. Cançado[1,4]

[1]*Divisão de Metrologia de Materiais, Instituto Nacional de Metrologia, Normalização e Qualidade Industrial (INMETRO), Duque de Caxias, RJ 25250-020, Brazil*

[2]*Departamento de Engenharia Metalúrgica e de Materiais, Universidade Federal do Rio de Janeiro, Rio de Janeiro, RJ 21941-972, Brazil*

[3]*Instituto de Física, Universidade Federal do Rio de Janeiro, Rio de Janeiro, RJ 21941-972, Brazil*

[4]*Departamento de Física, Universidade Federal de Minas Gerais, Belo Horizonte, MG 30123-970, Brazil*

[5]*Departamento de Física, Universidade Federal do Ceará, P. O. Box 6030, Fortaleza, CE 60455-760, Brazil*

[6]*Department of Physics, The Pennsylvania State University, University Park, Pennsylvania 16802, USA*

(Received 1 March 2013; revised manuscript received 26 June 2013; published 2 August 2013)

In this work, a study of resonance effects in the Raman spectra of twisted bilayer graphene (tBLG) is presented. The analysis takes into account the effect of the mismatch angle θ between the two layers, and also of the excitation laser energy on the frequency, linewidth, and intensity of the main Raman features, namely the rotationally induced R band, the G band, and the second-order G' (or $2D$) band. The resonance effects are explained based on the θ dependence of the tBLG electronic structure, as calculated by *ab initio* methodologies. The twist angle θ also defines the observation of a "D-like" band which obeys the double-resonance process, but relies on the superlattice along with long-range defects in order to fulfill momentum conservation. The study was possible due to the development of a route to produce and identify rotationally stacked bilayer graphene by means of atomic force microscopy (AFM).

DOI: 10.1103/PhysRevB.88.085401 PACS number(s): 78.30.−j, 68.65.Cd, 68.65.Pq

I. INTRODUCTION

Graphene is a honeycomb lattice made of carbon atoms at the hexagon vertices, whose unit cell is composed of two crystallographically inequivalent atoms, named A and B.[1] When two graphene layers are placed on top of each other, a superlattice structure (called Moiré pattern) generated by the mismatch rotation angle θ between the top and bottom layers is formed.[2] This superlattice is an in-plane periodic structure with lattice parameters ($\mathbf{r}_1$,$\mathbf{r}_2$) larger than graphene lattice parameters ($\mathbf{a}_1$,$\mathbf{a}_2$). While the electronic structure for monolayer graphene near the Fermi level shows a linear dispersive behavior, with a density of states (DOS) linearly increasing when departing from the neutrality point,[3] bilayer graphene with a twist angle θ presents two van Hove singularities (vHs's) in the DOS, one above and one below the Fermi level.[4] The energy difference between these vHs's (E_{vHs}) can be tuned by controlling the relative angle θ between layers. The presence of vHs's near the Fermi energy can generate electronic instabilities which are of great interest in materials science,[4–9] and the possibility to make and control these singularities open new paths for optoelectronic engineering of graphene-based devices.

Due to the peculiar electronic dispersion near the Fermi level, optical absorption in graphene is always resonant, and the Raman spectrum of graphene is remarkable for its strong resonant character.[10,11] Additionally, there are strong resonance processes associated with electron-phonon scattering involving vibrational modes with nonzero wave vectors q. For example, besides the single-resonance first-order Raman $q \approx 0$ active G band ($\sim$1584 cm^{-1}), the two-phonon G' (or $2D$) band centered at $\sim$2700 cm^{-1} (for a 514.5 nm excitation laser line) is originated from triple-resonance processes in monolayer graphene.[12,13] The G and G' bands have been largely used to study the electronic structure of graphene-based systems[10,11] including, more recently, the effects of graphene superlattice formation in twisted bilayer graphene (tBLG).[14–21] New Raman modes, named R (for rotation mismatch), emerge in tBLG, their frequencies depending on the rotational angle θ due to a special superlattice-activated Raman processes.[15–18]

This work presents several aspects related to resonance effects in the Raman spectra of tBLG. The analysis takes into account the effects of θ and excitation laser energy E_{L} on the frequency, linewidth, and intensity of the main Raman features, namely the superlattice-activated R band, the G band, the D band, and the second-order G' (or $2D$) band. The paper is organized as follows. In Sec. II a route for production of tBLG using an atomic force microscopy (AFM) tip is presented. Section III shows that one can probe the phonon dispersion of tBLG with Raman spectroscopy by changing the twist angle θ. Section IV discusses the strong resonance enhancement of the G band in tBLG for specific excitation laser energies, as reported in Refs. 14 and 19–21. Our experimental data reveals that the superlattice-activated R band presents the same enhancement, and a theoretical model is proposed to explain this resonance-based effect. The results are summarized in a simple analytical equation which directly relates the transition energy for maximum optical absorption to the twist angle θ. Section V presents a discussion on the presence of a "D-like" band, as first reported in Ref. 15. The comparison between the D-like band obtained from a tBLG and the disorder-induced D band obtained from a Ar^+-bombarded sample[22,23] confirmed that, although the D-like band shows the same frequency dispersion as the usual D band, the relative intensity between the D-like band and the G band does not follow the well-known proportionality with the inverse of the fourth power of the excitation laser energy.[24,25] These results are explained by considering that momentum conservation in the double-resonance process giving rise to the D-like band is

mediated by the static potential of superlattices with large twist angles ($\theta \rightarrow 30^\circ$) combined with long-range defects such as Coulomb impurities, intercalants, or strain. Section VI presents some resonance aspects related to the two-phonon G' band as follows: (i) the full width at half maximum (FWHM) of the G' band decreases by increasing θ; (ii) for samples with $\theta > 7^\circ$, the G' presents a considerably narrower profile than that observed in the Raman spectrum of undoped pristine monolayer graphene, the details being θ dependent, and (iii) the G' band in tBLG has approximately the same dispersion as obtained for undoped monolayer graphene. Section VII summarizes the main findings of the paper.

II. THE ROUTE TO PRODUCE FOLDED TWISTED BILAYER GRAPHENE

Figure 1(a) shows a tapping mode atomic force microscopy (AFM) image of a monolayer graphene obtained from the micromechanical exfoliation process applied to graphite flakes provided by *Nacional de Grafite Ltda.*, and deposited on top of a Si/SiO_2 substrate.[3] The method to produce folded tBLG starts with the generation of defective lines along a specific direction by scanning with the AFM tip several times over the same line [white arrows in Fig. 1(a)], applying a constant force. In sequence, the sample is scanned in contact mode with the fast scanning direction parallel to the graphene edge. This scanning process pushes the graphene edge towards the layer, thus inducing the folding by cutting the sheet preferentially where the defect lines were formerly created. The AFM image shown in Fig. 1(b) reveals three tBLGs with dimensions ranging from one to several microns produced by using this method. Notice that all these folds were intentionally made along the same direction in order to produce three tBLGs with same twist angle θ.

As discussed in Ref. 16, three folds with the same θ are expected to exhibit the same rotation-induced R band. The Raman image presented in Fig. 1(c) renders the G band intensity. This image identifies the positions of the tBLGs since the G band intensity is twice larger than that of monolayer graphene. Figure 1(d) shows the mapping of the R band ($\sim$1381 cm^{-1}) intensity, observed only at the tBLGs. Figure 1(e) shows the Raman spectra obtained from the three tBLGs shown in Fig. 1(b). All three spectra exhibit the same R band located at 1381 cm^{-1}, thus indicating a twist angle $\theta \simeq 27^\circ$.[16] This angle is confirmed here with lattice-resolution AFM measurement, as reported in Ref. 16. It can be seen in Fig. 1(e) that the R band is unusually narrow for a graphene-related Raman line (FWHM: $\Gamma_R \approx 4$ cm^{-1}), indicating that the wave vector of the created phonon is well defined by the superlattice. The peak observed at $\sim$1350 cm^{-1} is assigned as a D-like band.[15] We use the term "like" because, although this band occurs at similar frequencies and is related to the same TO phonons near the K point of graphene as the well-known defect-induced D band,[22,25] in the present case it is not induced by the same type of lattice defects. Its origin will be discussed further in Sec. V.

It should be mentioned that, besides the folding method described above, tBLG samples can be produced by other techniques. In fact, tBLG layers can occur naturally at the surface of crystalline graphite,[26] so that the mechanical exfoliation method, broadly used to produce graphene systems, can generate such structures naturally. Accidentally folding graphene into itself during the exfoliation procedure is also possible.[15] It has also been observed to occur unintentionally in graphene systems grown by CVD.[27–29] Other techniques, such as washing exfoliated graphene with a water flux, can be applied to increase the yield of graphene structures folded into themselves.[30] For sample characterization, besides the lattice-resolution AFM, high-resolution transmission electron microscopy (HRTEM) has also been used to independently assign the twist angle θ (e.g., Refs. 19, 20, and 31).

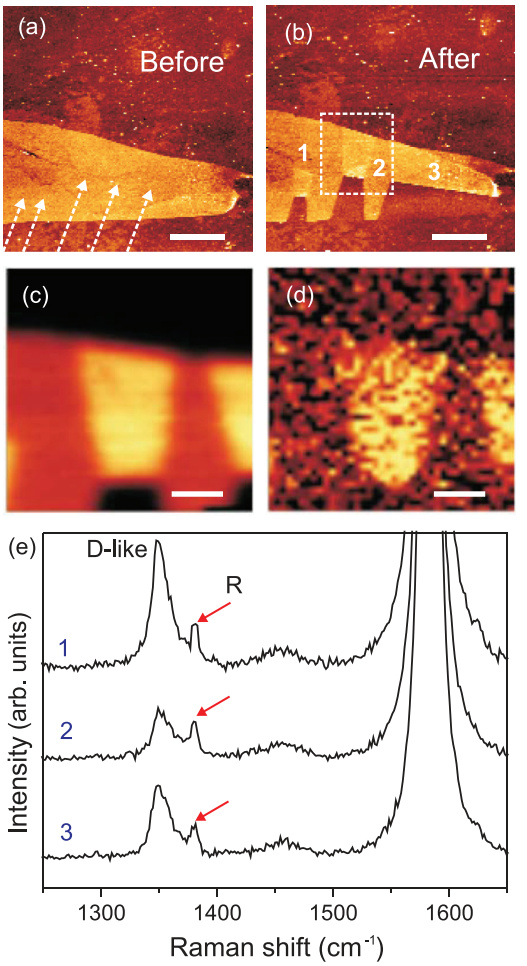

FIG. 1. (Color online) (a) AFM image of a monolayer graphene sitting on a Si/SiO_2 substrate. The white arrows indicate where defects were generated using the AFM tip in contact mode. The scale bar denotes 4 μm. (b) Three tBLGs obtained by AFM folding. The scale bar denotes 4 μm. (c) Mapping of the G band ($\sim$1580 cm^{-1}) intensity. The image was obtained from the boxed area in (b). The scale bar denotes 1 μm. (d) R band intensity ($\sim$1380 cm^{-1}) obtained simultaneously with the image shown in (c). The scale bar denotes 1 μm. (e) Raman spectra obtained from the three tBLGs shown in (b).

III. PROBING THE HIGH-FREQUENCY OPTICAL PHONON BRANCHES WITH THE R AND R' BANDS

The methodology described in Sec. II has been systematically performed to produce different well-defined Moiré patterns. Figure 2 shows the plot of the R' and R

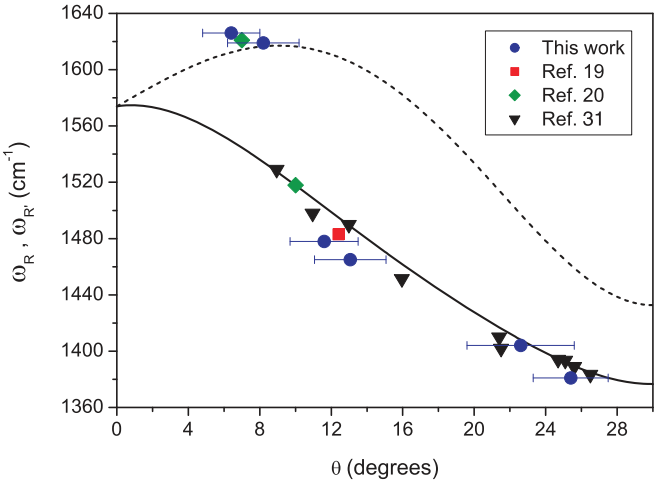

FIG. 2. (Color online) R' and R bands frequencies ($\omega_{R'}$ and ω_R, respectively) as a function of the twist angle θ. The solid circles with error bars present the data obtained from the overall set of samples produced in the current work. Other symbols are experimental data taken from Refs. 19, 20, and 31, as displayed in the legend.

bands frequencies ($\omega_{R'}$ and ω_R, respectively) as a function of the twist angle θ. The solid circles with error bars present the data obtained from the overall set of samples produced in the present work, with θ determined by means of lattice resolution AFM.[32] All other symbols are experimental data taken from literature (see legend in Fig. 2), with θ values determined by HRTEM. The upper (dashed) and lower (solid) curves are the theoretical dependencies of $\omega_{R'}$ and ω_R on θ, respectively, following the same procedures described in Ref. 16. Because they come from the LO and TO phonon branches, respectively, the R' and R bands have been named as R_{LO} and R_{TO} in Ref. 18.

IV. THE EXCITATION LASER ENERGY DEPENDENCE FOR THE G AND R BAND INTENSITIES

Recent theoretical and experimental works have reported the presence of van Hove singularities in the density of π electron states in tBLG.[4,8,33,34] References 14 and 19–21 have demonstrated that these vHs's induce very strong enhancement in the G band intensity, and that the maximum enhancement occurs for specific incident laser energies (E_L^{max}) defined by the twist angle θ, as shown in Fig. 3. Figure 3(a) depicts two Raman spectra obtained from the same graphene sample. Lattice-resolution AFM measurements revealed that this sample has a folded area with a twist angle $\theta = 13 \pm 3^\circ$. The upper spectrum was obtained from the folded area, while the bottom spectrum was obtained from the monolayer area. Although both spectra were measured under the same conditions (acquisition time, laser power density, and $E_L = 2.71$ eV), the G band obtained from the folded area is about 60 times more intense than the G band obtained from the single layer graphene area (G_{SLG}). Notice the presence of the R band centered at $\sim$1464 cm^{-1} in the Raman spectrum obtained from the folded area. Figures 3(b) and 3(c) show, respectively, the G and R bands obtained from the same tBLG as in Fig. 3(a), for six different values of E_L (1.96, 2.33, 2.41, 2.54, 2.71, and 3.81 eV). These two plots clearly show that not only the G, but also the R band intensity presents strong dependence on E_L, the maximum enhancement occurring at the same laser energy. Figures 3(d) and 3(e) show the normalized G and R bands intensities [$I(R)/I(G_{SLG})$ and $I(G)/I(G_{SLG})$, respectively] as a function of E_L. Data denoted by $\triangledown$ and $\blacktriangledown$ were obtained from tBLGs with $\theta = 12 \pm 2^\circ$ and $\theta = 13 \pm 3^\circ$, respectively. The R band frequencies observed for these two tBLGs were $\omega_R = 1464$ cm^{-1} ($\theta = 12^\circ$) and $\omega_R = 1478$ cm^{-1} ($\theta = 13^\circ$).

The G band enhancement in tBLG has been described by second order time-dependent perturbation in Ref. 21. The major contribution for the intensity comes from resonance matching between E_L and the separation of vHS's in the DOS of tBLG, that is, for $E_L = E_{vHs}$. Therefore, the E_L dependence of the normalized G band resonance profile shown in Fig. 3(d) can be evaluated as[10]

$$\frac{I(G)}{I(G_{SLG})} = \left| \frac{M}{(E_L - E_{vHs} - i\gamma)(E_L - E_{vHs} - \hbar\omega_G - i\gamma)} \right|^2, \quad (1)$$

where $\hbar\omega_G$ is the energy of the G phonon, and M is a constant that encompasses the product of the matrix elements for electron-photon and electron-phonon interactions. γ is the resonance window width, that is, the energy uncertainty related to the lifetime of the excited state. The solid and dashed lines in Fig. 3(d) are reconstructions according to Eq. (1), where the parameters E_{vHs}, M, and γ are obtained using a least-squares method. We found $E_{vHs} = 2.68$ and 2.79 eV, and $M = 0.105$ and 0.18, for the samples with twist angle $\theta = 12^\circ$ and $\theta = 13^\circ$, respectively. Within the experimental accuracy we found $\gamma = 0.12$ eV. In principle, the γ factors appearing at the denominator of Eq. (1) can be different to each other,[10] but we consider them to be the same here since we do not have experimental accuracy to differentiate them.

The R band intensity is described by third-order time-dependent perturbation since this process involves an additional interaction between the photoexcited electron (with wave vector k) and the periodic potential of the superlattice (associated with a wave vector q).[21] In this case, the normalized R band intensity is given as

$$\frac{I(R)}{I(G_{SLG})} = \left| \frac{M'}{(E_L - E_{vHs} - i\gamma)[E_L - E_{eh}(k+q) - i\gamma](E_L - E_{vHs} - \hbar\omega_R - i\gamma)} \right|^2, \quad (2)$$

where $E_{eh}(k+q)$ is the electron-hole pair state energy at $k+q$. For E_L in the visible range, the term between brackets in the denominator of Eq. (2) plays a minor role in the resonance profile because (i) E_L is far from $E_{eh}(k+q)$, so this is not a diverging term and (ii) it is a smooth function of E_L in the measured range. As discussed in Ref. 16, for $\theta > 8^\circ$ this term

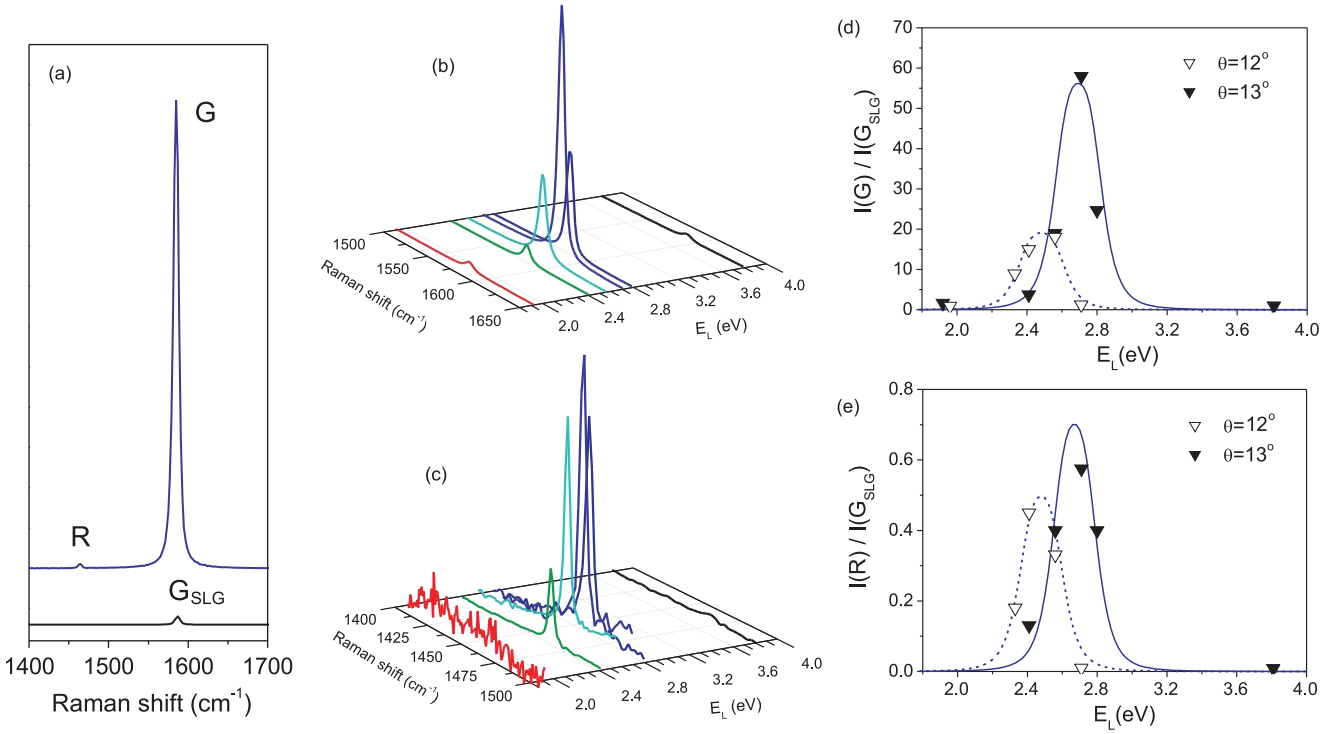

FIG. 3. (Color online) (a) Raman spectra obtained from a graphene with a folded area with $\theta = 13 \pm 3^\circ$, according to lattice-resolution AFM measurements. The upper (lower) spectrum was obtained from the folded (unfolded) area. (b) and (c) G and R band spectra of the same tBLG showed in (a) for six different values of E_L. (d) and (e) Normalized G and R bands intensities [$I(G)/I(G_{SLG})$ and $I(R)/I(G_{SLG})$, respectively] as a function of E_L. Data denoted by ▽ and ▼ were obtained from tBLGs with $\theta = 12 \pm 2^\circ$ and $\theta = 13 \pm 3^\circ$, respectively. The lines are plots according to Eqs. (1) and (2) (see detailed discussion in the text).

will become important for excitation laser energies in the UV range, for which a possible match between E_L and $E_{eh}(k+q)$ can give rise to a double-resonance condition. Since the R band resonance profiles measured here were obtained for E_L in the visible range, this term can be disregarded in the fitting. This procedure was carried out for the data depicted in Fig. 3(e) (solid and dashed lines), and we found that the R band resonance profile is well described by the same values of E_{vHs} and γ obtained for the respective G band data shown in Fig. 3(d). We found $M = 0.016$ and 0.019 for the samples with twist angle $\theta = 12^\circ$ and $\theta = 13^\circ$, respectively.

Figure 4 presents a summary of the literature experimental data (open symbols) and theoretical results for the G band enhancement in tBLG. The graphics shows the plot of the incident laser energy for maximum enhancement (E_L^{max}) as a function of the twist angle θ. The solid circles with error bars are our experimental data obtained from the fit-parameter E_{vHs} in Fig. 3(d) (notice that $E_{vHs} = E_L^{max}$). The dot-dashed and dashed lines in Fig. 4 are the theoretical models proposed in Refs. 19 and 20, respectively. Solid triangles are theoretical results from Ref. 21. While Ref. 14 proposed a double-resonance mechanism involving intralayer and parallel transitions, Ref. 20 proposed that the G band enhancement is originated from intralayer electronic transitions connecting vHs's in the electronic DOS. The model presented in Ref. 19 is based on electronic transitions between parallel bands giving rise to a large joint DOS. According to the authors, the Raman process originated from these parallel band transitions add coherently for the total resonance Raman intensity. Reference 21 evaluated the resonance G band intensity in tBLG considering the electron-photon and electron-phonon matrix elements, and the authors observed the occurrence of

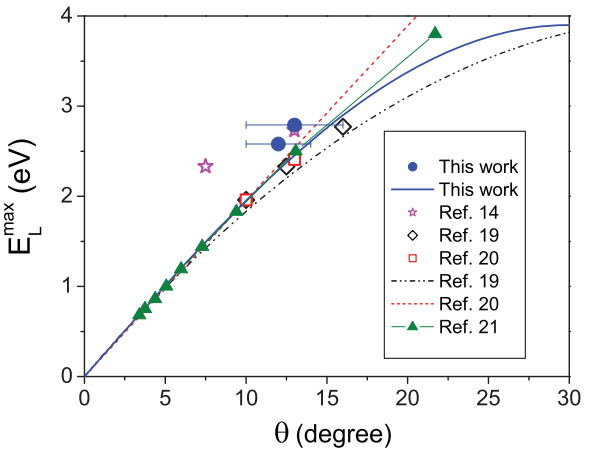

FIG. 4. (Color online) Summary of the literature experimental data (open symbols) for the G band enhancement in tBLG. The graphic shows the plot of the excitation laser energy that activates the maximum enhancement process ($E_L^{max} = E_{vHs}$) as a function of θ. The dot-dashed and dashed lines are the theoretical models proposed in Refs. 19 and 20, respectively. Solid triangles are theoretical calculations from Ref. 21. The solid line is our theoretical result. The solid circles with error bars are our experimental data obtained from the fit parameters in Fig. 3(d).

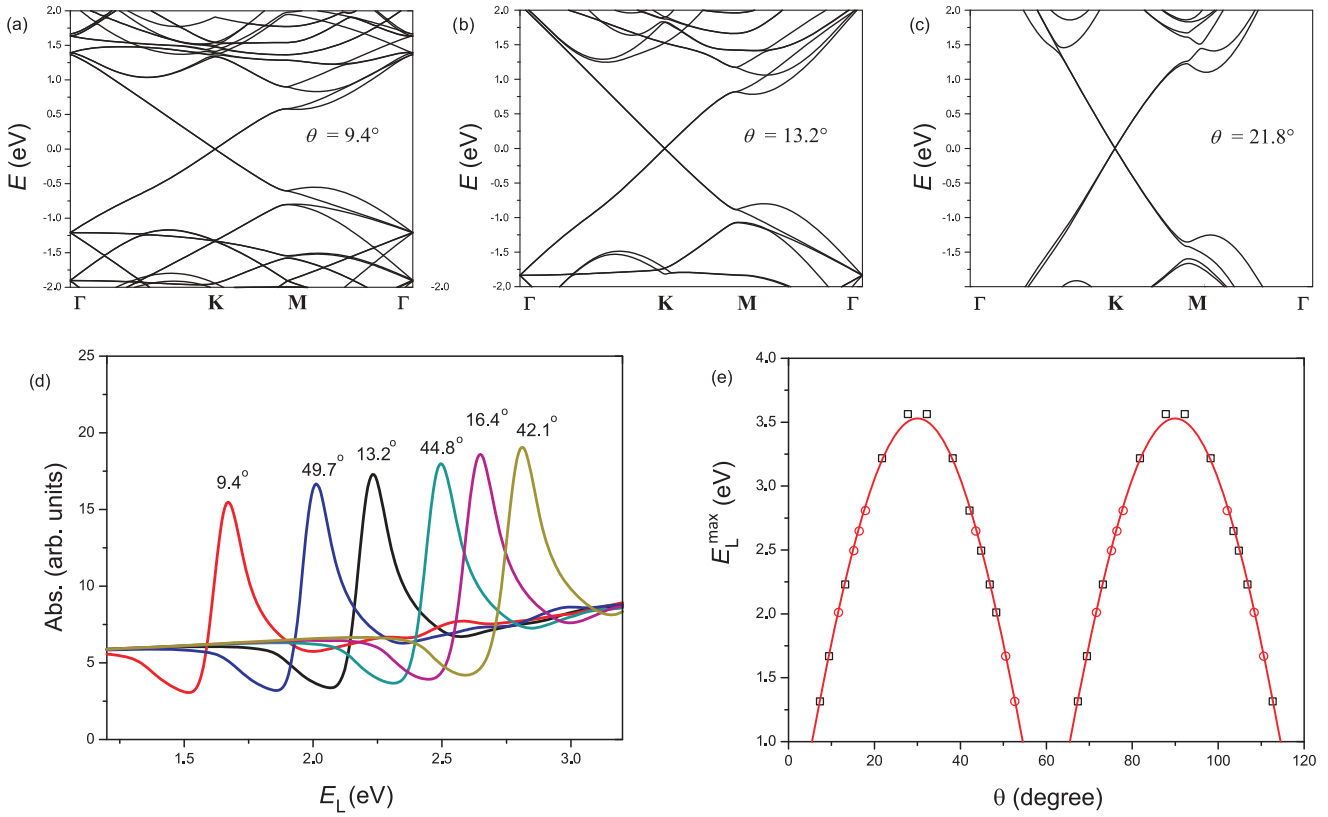

FIG. 5. (Color online) Calculated electronic and optical properties of tBLG. (a)–(c) Electronic structure for three distinct rotation angles θ (namely 9.4°, 13.2°, and 21.8°, respectively). (d) Calculated optical absorption spectra for six different values of θ which are displayed near each respective absorption peak. (e) θ dependence for the optical absorption peaks at $E_{\mathrm{L}}^{\max}$, according to the results shown in (d), and others not shown. □ are calculated data, ◯ are values replicated by symmetry, and the solid line is given by Eq. (3).

peaks in the JDOS due to electronic vHs coming from band structure features in the vicinity of the M point of the Brillouin zone, giving rise to strong optical absorption.

In order to check the influence of the optical absorption on the G and R bands intensities, we performed *ab initio* calculations for the electronic structure of tBLG (see Fig. 5). All calculations were performed within LDA-DFT formalism using the computational package SIESTA.[35] We used a $30/T \times 30/T \times 1$ k-points grid in the self-consistent calculation, where $T = \sqrt{n^2 + nm + m^2}$ is the magnitude of the (n,m) supercell vectors with respect to the graphene lattice parameter $a = 2.465$ Å. The separation c between two graphene layers varies with θ in the range $0° < \theta < 60°$, and has a different value from the AA ($\theta = 60°$ and $c_{\mathrm{AA}} = 3.456$ Å) and AB ($\theta = 0°$ and $c_{\mathrm{AB}} = 3.178$ Å) stacking. Therefore, for all tBLGs different from the AA and AB stacking, we used a fixed value for $c_{\mathrm{twist}} = 3.29$ Å obtained from the average value given by energy minimization. The results are depicted in Figs. 5(a)–5(c), which show the electronic band structures of tBLGs with three distinct rotation angles θ (namely 9.4°, 13.2°, and 21.8°, respectively).

We then analyze the optical absorption spectrum constructed using dipole transition matrix elements between valence and conduction Kohn-Sham states. In this calculation, we used a grid with $400/T \times 400/T \times 1$ k points for energies up to 4 eV using an in-plane electric field polarization. The absorption spectrum was then smoothed by Gaussian functions with width of 0.05 eV, and the optical transition energies were enhanced by 18% to account for quasiparticle effects, as suggested in Ref. 20. Figure 5(d) shows the calculated absorption spectra for six values of θ. Notice that for a given value of θ, one very well-defined absorption peak is observed. The values for the resonance transition energy $E_{\mathrm{L}}^{\max}$ as a function of θ calculated by DFT (increased by 18%) are plotted as open squares in Fig. 5(e). The open circles represent values replicated by symmetry since $E_{\mathrm{L}}^{\max}$ is expected to be symmetrical around $\theta = 30°$ and periodic at 60°. Our results can be fitted as

$$E_{\mathrm{L}}^{\max} = E_0 |\sin(3\theta)|, \tag{3}$$

with $E_0 = 3.9$ eV. The maximum energy absorption occurs exactly at $\theta = 30°$, for which the largest possible separation between Dirac points occurs. The full θ dependence shown in Fig. 5(e) has been translated into the solid line in Fig. 4. Again, it is important to emphasize that the enhancement of the R band at laser energies given by Eq. (3) is solely driven by the electron-photon matrix element and therefore it occurs independently and in addition to the double-resonance condition discussed in Ref. 16, which gives rise to R-band enhancement for yet other values of laser energy.

It should be noticed that Eqs. (1) and (2) are approximations since the complete calculation should include the summation over all intermediate states, rather than a single level state at the van Hove singularity. However, the effect of considering all

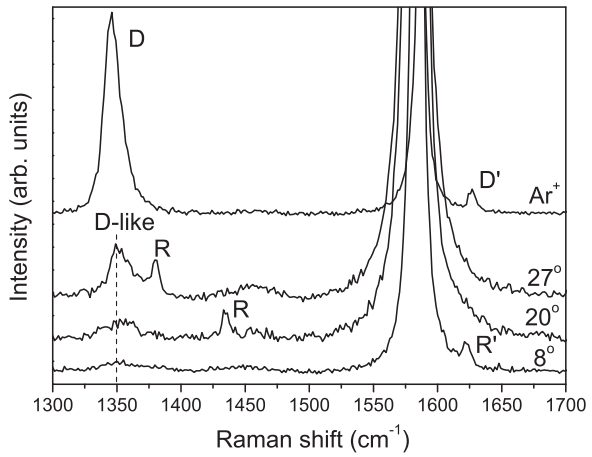

FIG. 6. From the bottom: Raman spectra of three tBLGs with $\theta = 8°$, 20°, and 27°, respectively. The upper spectrum was obtained from an Ar^+-bombarded monolayer graphene. All data were obtained with $E_L = 2.41$ eV.

intermediated states would be a broadening in the resonance profile, which was not observed in the fitting procedure, thus showing that the simplified Eqs. (1) and (2) can be used to a first approximation.

V. THE "*D*-LIKE" BAND IN tBLG

Figure 6 shows the Raman spectra of three tBLGs ($\theta = 8°$, 20°, and 27°; bottom spectra), obtained using $E_L = 2.41$ eV. The upper spectrum was obtained from an Ar^+-bombarded monolayer graphene.[22] The ion-bombardment procedure generates pointlike defects that activate the disorder-induced D band centered at ~1350 cm^{-1} for $E_L = 2.41$ eV. The value of the ratio between the D and G bands intensities [$I(D)/I(G) = 0.5$] indicates a defect density of $n_D \simeq 1.2 \times 10^{11}$ cm^{-2}.[22,25] The D band is also present in the Raman spectrum of the tBLG with $\theta = 27°$ [see Figs. 1(e) and 6], although this sample does not present a considerable amount of structural defects, as indicated by the Raman spectrum obtained from the unfolded area (not shown here). Therefore, the observation of the D-like band is associated with the static potential, as proposed by Gupta *et al.*[15] Notice from Fig. 6 that the Raman spectrum of the tBLG with $\theta = 20°$ has a considerably weaker D-like band, and for the tBLG with $\theta = 8°$ the D-like band is almost undetectable. The D' band (present in the Raman spectrum obtained from the Ar^+-bombarded monolayer graphene) was not observed in the Raman spectrum of the tBLG with $\theta = 27°$.

To prove that the D-like band comes from the tBLG, we performed Raman imaging experiments. Figure 7(a) shows the topographic image of a tBLG obtained by the folding method described in Sec. II. Figures 7(b) and 7(c) show the G and D band intensity maps, respectively, obtained from the tBLG shown in Fig. 7(a). As shown in Fig. 7(b), the G band intensity is twice larger in the folded area, as expected. For the D band [Fig. 7(c)], its intensity is stronger at the edges of the tBLG, and non-null at the inner area. Inside the tBLG area, the D-like band presents homogeneous intensity distribution. This is clearly observed in the intensity profile shown in Fig. 7(d), obtained along the dashed line depicted

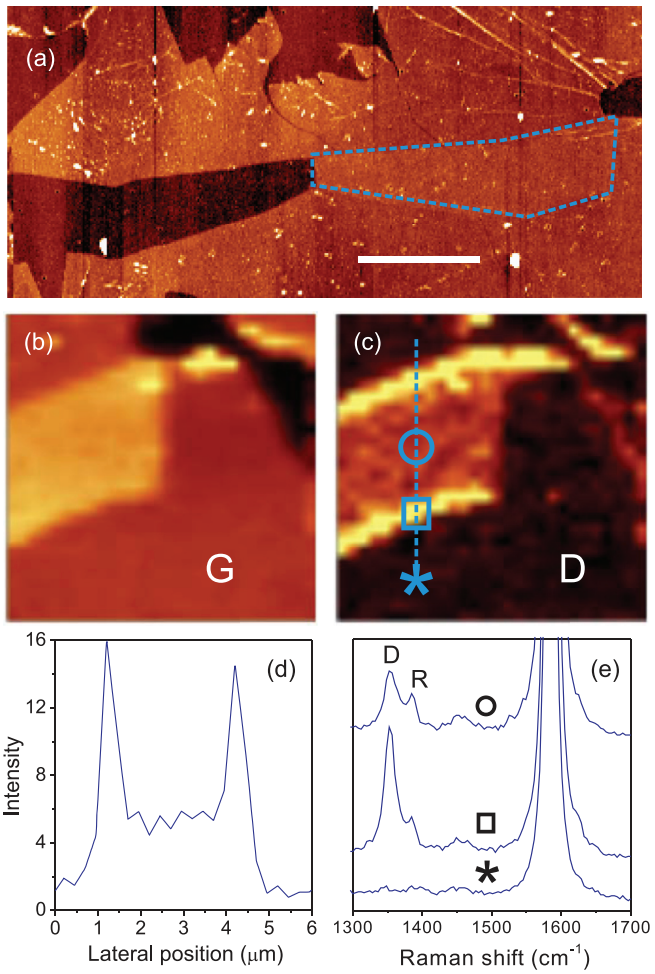

FIG. 7. (Color online) (a) Topographic image of a SLG sample. The dashed line highlights a tBLG obtained by the folding method described in Sec. II. The scale bar denotes 5 μm. (b) and (c) G and D band intensity maps, respectively, obtained from the tBLG shown in (a). In both cases, the images lateral size is 7 μm. (d) D band intensity profile obtained along the dashed line in (c). (e) Raman spectra taken from the marked regions in (c) (□ from the tBLG edge, ◯ from the tBLG inner area, and ∗ from the SLG near it). The R band centered at ~1380 cm^{-1} observed in the spectra obtained from the tBLG indicates a twist angle $\theta \simeq 27°$. All Raman data displayed in this figure were acquired with the electric field of the incident laser polarized along the horizontal direction as defined in (a)–(c), that is, roughly parallel to the tBLG edges.

in Fig. 7(c). In Fig. 7(e) we have three spectra taken from the marked regions in Fig. 7(c) (□ from the tBLG edge, ◯ from the tBLG inner area, and ∗ from the SLG near it). The R band centered at ~1380 cm^{-1} observed in the spectra obtained from the tBLG indicates a twist angle $\theta \simeq 27°$. The data displayed in Figs. 7(c) and 7(e) show that the D-like band undoubtedly arises from the tBLG area, and cannot be attributed to edge defects.

Figure 8(a) shows four Raman spectra of a tBLG with $\theta = 27°$ (the same shown in Fig. 7), each one obtained with a distinct excitation laser energy ($E_L = 1.92$, 2.41, 2.71, and 3.81 eV). We also performed similar measurements (spectra not shown here) on the Ar^+-bombarded SLG sample with $n_D \simeq 1.2 \times 10^{11}$ cm^{-2}, for comparison. Figure 8(b) shows

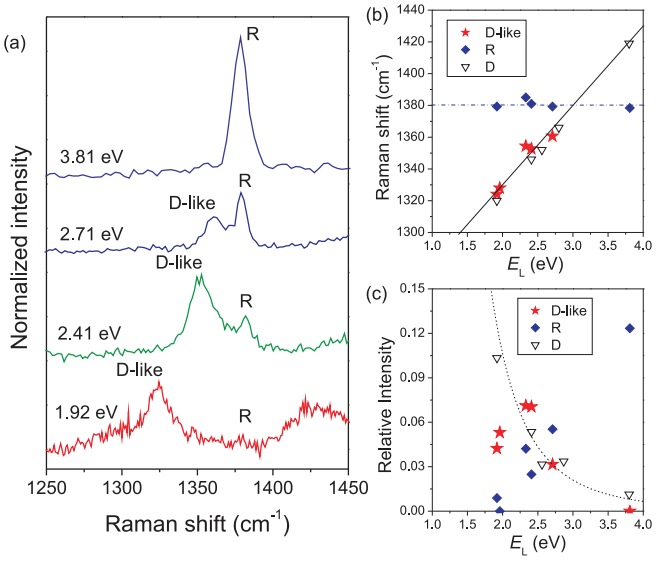

FIG. 8. (Color online) (a) Raman spectra of a tBLG with $\theta = 27^\circ$ (the same shown in Fig. 7), obtained with four distinct excitation laser energies ($E_L = 1.92$, 2.41, 2.71, and 3.81 eV). All spectra were normalized by the intensity of the G band obtained from the unfolded area (G_{SLG}). (b) Frequency (Raman shift) of the D-like (stars), and R (diamonds) bands for $E_L = 1.92$, 1.96, 2.33, 2.41, 2.71, and 3.81 eV. The solid line is a linear fit yielding $\omega(D\text{-like}) = 1230\ \text{cm}^{-1} + 50\ \text{cm}^{-1}/\text{eV}$, where $\omega(D\text{-like})$ is the frequency of the D-like band. The down-open triangles show the frequency of the D band obtained from a Ar$^+$-bombarded SLG sample with $n_D \simeq 1.2 \times 10^{11}\ \text{cm}^{-2}$, for $E_L = 1.92, 2.41, 2.54, 2.8$, and 3.81 eV. (c) Normalized intensity [the intensity divided by $I(G_{SLG})$] of the D-like (stars) and R (diamonds) bands for $E_L = 1.92$, 1.96, 2.33, 2.41, 2.71, and 3.81 eV. The open-down triangles show the $I(D)/I(G)$ ratio (divided by 10 for better visualization) of the Ar$^+$-bombarded SLG sample with $n_D \simeq 1.2 \times 10^{11}\ \text{cm}^{-2}$ for $E_L = 1.92$, 1.96, 2.33, 2.41, 2.71, and 3.81 eV. The dashed line is the plot of $I(D)/I(G) = n_D/[(7.3 \times 10^9)E_L^4]$.[25]

the frequency (Raman shift) of the D (obtained from the Ar$^+$-bombarded SLG), D-like, and R bands (both obtained from the tBLG with $\theta = 27^\circ$) as a function of E_L. As depicted in the plots, the D and D-like bands present a similar dispersion of $\sim 50\ \text{cm}^{-1}/\text{eV}$, which is the typical value for the D band double-resonance dispersion.[36] This data shows that the D-like band is associated with TO phonons near the K point, as for the D band, and obey double-resonance frequency behavior. On the other hand, the R band does not show a detectable dispersion. As explained in Ref. 16, the R band is not dispersive because the wave vector ($\mathbf{q}_R$) of the TO phonon created in the Raman process (considering Stokes processes) is uniquely determined by the superlattice wave vector $\mathbf{q}$, being $\mathbf{q}_R = -\mathbf{q}$.

Figure 8(c) shows the normalized intensity [the intensity divided by $I(G_{SLG})$] of the D (obtained from the ion-bombarded sample), D-like, and R bands as a function of E_L. As shown in the figure, the relative intensity of the R band [$I(R)/I(G_{SLG})$] increases by increasing E_L, reaching a maximum value for $E_L = 3.81$ eV, consistent with the theory proposed in Ref. 16 and the resonance model displayed in Eq. (2). The ratio between the D and G bands obtained from the ion-bombarded sample follows the well-known relation

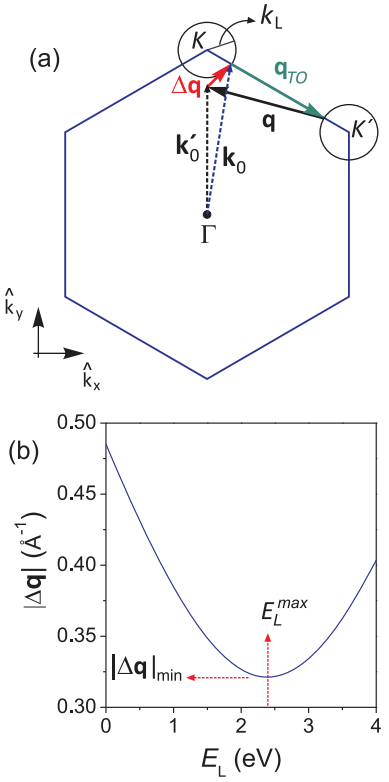

FIG. 9. (Color online) (a) The first Brillouin zone of graphene with the schematics of the scattering process giving rise to the D-like band. (b) Modulus of $\Delta\mathbf{q}$ [evaluated from Eq. (6)] as a function of the excitation laser energy E_L for $\theta = 27^\circ$.

$I(D)/I(G) \propto E_L^{-4}$ [dashed line in Fig. 8(c)].[24,25] On the other hand, the $I(D\text{-like})/I(G_{SLG})$ ratio follows a different trend, being maximum at approximately 2.4 eV and undetectable at 3.81 eV. These results drive us to a model that can explain the D-like band behavior, which is based on both superlattice and double-resonance effects.

Figure 9(a) shows the first Brillouin zone of graphene with the schematics of the scattering process giving rise to the D-like band, which starts with a photon of energy E_L being absorbed to generate an electron-hole pair. Considering that (i) the incident photon has been resonantly absorbed, (ii) the π electrons in tBLG have a linear energy dispersion in the range of optical transitions, and (iii) the π electron energy is isotropic around the K point, the photoexcited electron with wave vector $\mathbf{k}_0$ will belong to an equienergy circle around the K point with radius $k_L = E_L/2\hbar v_F$ [see Fig. 9(a)], where v_F is the Fermi velocity in graphene ($\sim 10^6$ m/s). The photoexcited electron is then inelastically scattered from the excited π^* state with energy $\epsilon(\mathbf{k}_0) = E_L/2$ to another π^* state (near the K' point) with energy $\epsilon(\mathbf{k}_0 + \mathbf{q}_{TO}) = E_L/2 - \hbar\omega_D$, by a phonon with wave vector $-\mathbf{q}_{TO}$ and frequency ω_D. As depicted in Fig. 9(a), we are considering inner scattering processes (connecting two π^* electron states along the K-K' line) that, according to recent theoretical calculations, dominates the double-resonance process.[13] Taking into account that $\hbar\omega_D$ is two orders of magnitude lower than E_L (for processes using laser lines in the visible range), the wave vector $\mathbf{q}_{TO}$ that provides the resonance condition for the transition between

these two intermediate states can be approximated by

$$\mathbf{q}_{\mathrm{TO}} \simeq \left(\frac{2\pi}{\sqrt{3}a} - \sqrt{3}\frac{E_{\mathrm{L}}}{2\hbar v_{\mathrm{F}}}\right)\hat{\mathbf{k}}_x + \left(\frac{E_{\mathrm{L}}}{2\hbar v_{\mathrm{F}}} - \frac{2\pi}{3a}\right)\hat{\mathbf{k}}_{\mathrm{y}}, \quad (4)$$

where $a = 2.46$ Å is the lattice parameter of graphene, and $\hat{\mathbf{k}}_{\mathrm{x}}$ and $\hat{\mathbf{k}}_{\mathrm{y}}$ are unit wave vectors as defined in Fig. 9(a). In the sequence, the electron must recombine with the hole to end the scattering process with the emission of a photon with energy $E_{\mathrm{L}} - \hbar\omega_{\mathrm{D}}$. However, momentum conservation is only achieved if the electron is backscattered to its initial wave vector $\mathbf{k}_0$ near the K point. In the case of the double-resonance process giving rise to the usual disorder-induced D band, the electron is elastically scattered by a lattice defect that provides the necessary "extra" momentum. For the D-like band in tBLG, the additional momentum is partially provided by the periodic potential of the superlattice with Fourier component at the wave vector $\mathbf{q}$, which is related to the rotational angle θ by

$$\mathbf{q}(\theta) = \frac{2\pi}{\sqrt{3}a}\{[-(1-\cos\theta) - \sqrt{3}\sin\theta]\hat{\mathbf{k}}_x + [-\sqrt{3}(1-\cos\theta) + \sin\theta]\hat{\mathbf{k}}_y\}. \quad (5)$$

However, as depicted in Fig. 9(a), the $\mathbf{q}$ wave vector is still not able to completely fulfill the momentum conservation condition for any specific value of E_{L} in the inner double-resonance process, since the electron is not backscattered to $\mathbf{k}_0$. In other words, at any angle θ, the periodical potential does not have a Fourier component with wave vector $\mathbf{q} = -\mathbf{q}_{\mathrm{TO}}$, able to scatter the electron back to $\mathbf{k}_0$. Instead, the electron is scattered by the periodical potential to a state with wave vector $\mathbf{k}_0'$. Therefore, the achievement of an inner double-resonance process giving rise to the D-like band in tBLG requires the presence of defects able to transfer a momentum $\hbar\Delta\mathbf{q}$ that satisfy the condition $\Delta\mathbf{q} + \mathbf{q} = -\mathbf{q}_{\mathrm{TO}}$ [see Fig. 9(a)].

It has been recently shown that the D band intensity strongly depends on the nature of the defects that provide momentum conservation in the double-resonance process.[13,37] Because the D band originates from intervalley scattering processes [the electron is scattered from a state near the K (or K') point to another state near the K' (or K) point], momentum conservation is mediated by localized defects (in the real space) such as armchair edges or vacancies, for which the short-range defect potentials are able to provide large momentum transfer, associated with wave vectors lying at the frontiers of the first Brillouin zone. As shown by the absence of D band in the unfolded region of our samples (see Fig. 7), such defects are not present in them. On the other hand, delocalized defects such as Coulomb impurities, intercalants, or strain have Fourier components only at relatively small wave vectors in the reciprocal space, close to the Γ point.[13,37] As depicted in Fig. 9(a), by taking into account the superlattice wave vector $\mathbf{q}$, the D-like band scattering only requires the presence of these defects, which can provide relatively small momentum transfer. Therefore, the D-like band is generated by the unavoidable presence of long-range defects such as charged impurities absorbed at the tBLG's surface,[38–40] intercalants,[41,42] or by strain induced during the superlattice formation.[43,44] Assuming a broad distribution of defect potential range, as short as $\Delta\mathbf{q}$ takes, more and more of those delocalized defects are able to deliver the necessary momentum for the activation of the D-like double-resonance process, so the intensity of the D-like band should increase as $|\Delta\mathbf{q}|$ decreases. By taking $\mathbf{q}_{\mathrm{TO}}$ and $\mathbf{q}$ from Eqs. (4) and (5), this wave vector $\Delta\mathbf{q}$ can be evaluated as

$$\Delta\mathbf{q} = \left(\sqrt{3}\frac{E_{\mathrm{L}}}{2\hbar v_{\mathrm{F}}} - \frac{2\pi}{\sqrt{3}a}\cos\theta + \frac{2\pi}{a}\sin\theta\right)\hat{\mathbf{k}}_{\mathrm{x}} + \left(\frac{8\pi}{3a} - \frac{E_{\mathrm{L}}}{2\hbar v_{\mathrm{F}}} - \frac{2\pi}{a}\cos\theta - \frac{2\pi}{\sqrt{3}a}\sin\theta\right)\hat{\mathbf{k}}_{\mathrm{y}}. \quad (6)$$

Figure 9(b) shows the modulus of $\Delta\mathbf{q}$ [evaluated from Eq. (6)] as a function of the excitation laser energy E_{L} for $\theta = 27^\circ$. Notice that $|\Delta\mathbf{q}|$ has a minimum value at $E_{\mathrm{L}}^{\max} \simeq 2.4$ eV. According to the experimental data depicted in Fig. 7(b), the normalized D-like band intensity shows a maximum for $E_{\mathrm{L}} = 2.41$ eV, indicating that, indeed, the D-like band exhibits a maximum relative intensity for minimum $|\Delta\mathbf{q}|$.

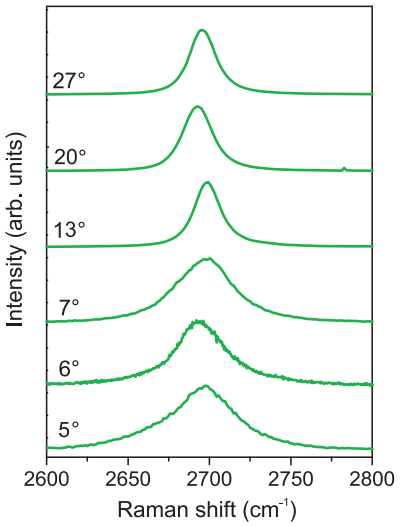

FIG. 10. (Color online) G' band in the Raman spectra of tBLGs with different values of θ. All spectra were obtained using $E_{\mathrm{L}} = 2.41$ eV.

VI. THE TWO-PHONON G' BAND IN tBLG

Figure 10 shows the G' band in the Raman spectra of tBLGs with different values of θ, measured by lattice-resolution AFM. All spectra were obtained using $E_{\mathrm{L}} = 2.41$ eV. For small rotation angles ($\theta \leqslant 7^\circ$), the G' band exhibits a complex line shape, which is asymmetric or composed by multiple peaks. For $\theta > 7^\circ$, the G' band changes to a single Lorentzian peak with FWHM around 23 cm^{-1}. This value is smaller than the usual FWHM of the G' band observed in the Raman spectrum of undoped pristine monolayer graphene (∼28–30 cm^{-1}).[38]

In order to check for the resonance properties of the G' band, we have measured the Raman spectra of tBLGs with $\theta = 5^\circ$, 13°, 20°, and 27°, using different excitation laser lines ($E_{\mathrm{L}} = 1.92$, 2.41, 2.54, 2.71, 2.8, and 3.81 eV). Figure 11(a) shows the FWHM of the G' band ($\Gamma_{G'}$) as a function of E_{L} for tBLGs with the different values of θ. As shown in the graphics, $\Gamma_{G'}$ increases as E_{L} increases for all tBLGs. However, except for $E_{\mathrm{L}} = 3.81$ eV, $\Gamma_{G'}$ obtained from the tBLG with $\theta = 5^\circ$ is considerably larger than for the

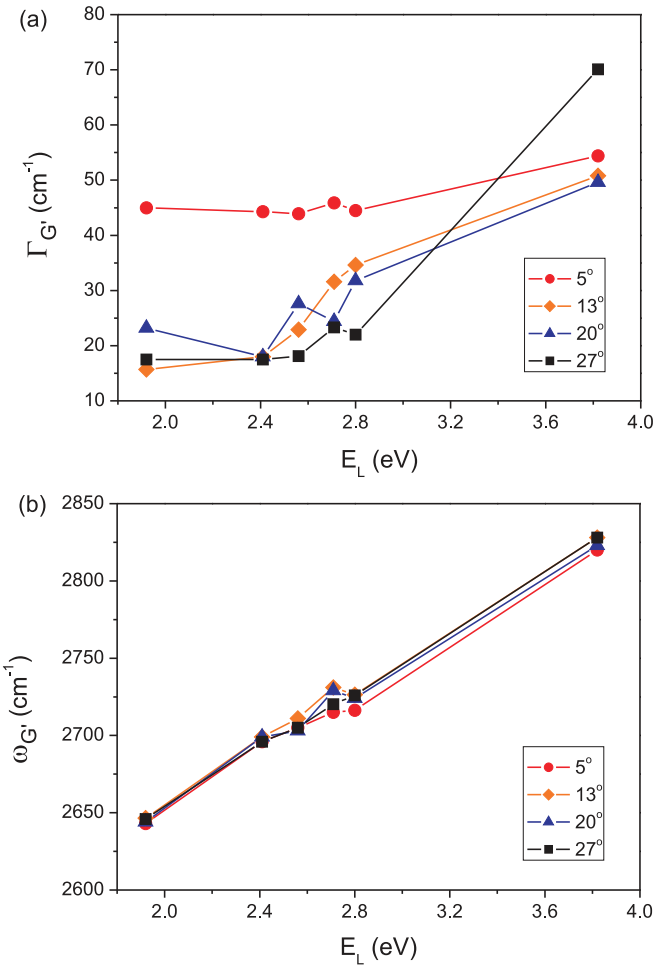

FIG. 11. (Color online) (a) FWHM of the G' band ($\Gamma_{G'}$) as a function of E_L for tBLGs with different values of θ. (b) Frequency (Raman shift) of the G' band ($\omega_{G'}$) as a function of E_L for different values of θ (see legend).

tBLGs with larger values of θ. This effect has been studied in Ref. 20, where the authors performed theoretical calculations showing that the dependence of the G' band profile on θ is related to the influence of interplane interactions on the electronic structure of tBLGs. Interestingly, the TO phonon dispersion is not considerably affected by this interplane interaction. This conclusion comes from Fig. 11(b), which shows the frequency (Raman shift) of the G' band ($\omega_{G'}$) as a function of E_L for $\theta = 5°$, 13°, 20°, and 27°. All tBLGs measured here presented approximately the same dispersion of $\sim$94 cm^{-1}/eV, which is similar to the dispersion obtained for undoped pristine monolayer graphene.[10] The influence of the interplane interactions are minor and located around 2.8 eV. The details might depend on θ, as discussed in Ref 20, and similar effect has been seen in single-wall carbon nanotubes, as discussed in Ref. 45.

VII. CONCLUSIONS

This work explores the resonance effects in the Raman spectrum of twisted bilayer graphene (tBLG), taking into account the influence of the incident laser energy (E_L) on the frequency, linewidth, and intensity of its main Raman features. The tBLGs used in this work were produced by folding a monolayer graphene over itself using an atomic force microscopy (AFM) tip.

The rotationally induced R band presents the same resonance enhancement previously observed for the G band in Refs. 14, 19, and 20, along with the double-resonance discussed in Ref. 16. Our results are explained by first-principles DFT calculations of optical absorption spectra of tBLG, and are summarized by a simple relation that gives the transition energy for maximum optical absorption as a function of the twist angle θ (E_L^{max}(eV) $= 3.9|\sin(3\theta)|$).

We studied a D-like band in the Raman spectra of tBLGs. Raman imaging of a tBLG with $\theta = 27°$ shows that the D-like band cannot be attributed neither to edges nor to vacancies. We propose that the D-like band is not activated by the same type of short-range lattice defects as the D band, but by a combination between the periodical potential of the superlattice in tBLGs with large θ angles (close to 30°) and long-range defects such as Coulomb impurities, intercalants, or strain. Therefore, the presence of a superlattice allows us to use Raman spectroscopy to investigate a class of defects in graphene-type samples which would not be accessible otherwise. Resonance aspects related to the two-phonon G' band were also discussed, and the dependencies of its frequency and linewidth on E_L and θ were explored.

ACKNOWLEDGMENTS

This work was financed by Inmetro, FAPERJ, and Rede Brasileira de Pesquisa e Instrumentação em Nano-Espectroscopia Óptica (CNPq/MCTI). A.J. and L.G.C. acknowledge Universal Grant CNPq, and FAPEMIG (Brazil). L.G.C. acknowledges the Grant PRONAMETRO (52600.056330/2012). V.C., B.F., and P.M.B. acknowledge the Grant CNPq/Prometro (563064/2010-2). R.B.C. acknowledges the Instituto Nacional de Ciência e Tecnologia (INCT) em Nanomateriais de Carbono - MCT, CNPq, and FAPEMIG (Brazil). A.G.S.F. acknowledges support from FUNCAP (PRONEX Processo 220100/11). We acknowledge M. S. C. Mazzoni for fruitful discussions.

[1]P. R. Wallace, Phys. Rev. **71**, 622 (1947).
[2]E. J. Mele, Phys. Rev. B **81**, 161405 (2010).
[3]K. S. Novoselov, A. K. Geim, S. V. Morozov, D. Jiang, Y. Zhang, S. V. Dubonos, I. V. Grigorieva, and A. A. Firsov, Science **306**, 666 (2004).
[4]G. Li, A. Luican, J. M. B. Lopes dos Santos, A. H. Castro Neto, A. Reina, J. Kong, and E. Y. Andrei, Nat. Phys. **6**, 109 (2010).
[5]W. Kohn and J. M. Luttinger, Phys. Rev. Lett. **15**, 524 (1965).
[6]T. M. Rice and G. K. Scott, Phys. Rev. Lett. **35**, 120 (1975).
[7]M. Fleck, A. M. Oles, and L. Hedin, Phys. Rev. B **56**, 3159 (1997).
[8]J. M. B. Lopes dos Santos, N. M. R. Peres, and A. H. Castro Neto, Phys. Rev. Lett. **99**, 256802 (2007).
[9]J. González, Phys. Rev. B **78**, 205431 (2008).

[10]A. Jorio, M. Dresselhaus, R. Saito, and G. Dresselhaus, *Raman Spectroscopy in Graphene Related Systems* (Wiley-VCH, Berlin, 2011) .
[11]R. Saito, M. Hofmann, G. Dresselhaus, A. Jorio, and M. S. Dresselhaus, Adv. Phys. **60** (2011).
[12]D. M. Basko, Phys. Rev. B **76**, 081405 (2007).
[13]P. Venezuela, M. Lazzeri, and F. Mauri, Phys. Rev. B **84**, 035433 (2011).
[14]Z. Ni, L. Liu, Y. Wang, Z. Zheng, L.-J. Li, T. Yu, and Z. Shen, Phys. Rev. B **80**, 125404 (2009).
[15]A. K. Gupta, Y. Tang, V. H. Crespi, and P. C. Eklund, Phys. Rev. B **82**, 241406 (2010).
[16]V. Carozo, C. M. Almeida, E. H. M. Ferreira, L. G. Cançado, C. A. Achete, and A. Jorio, Nano Lett. **11**, 4527 (2011).
[17]A. Righi, S. D. Costa, H. Chacham, C. Fantini, P. Venezuela, C. Magnuson, L. Colombo, W. S. Bacsa, R. S. Ruoff, and M. A. Pimenta, Phys. Rev. B **84**, 241409 (2011).
[18]J. Campos-Delgado, L. G. Cançado, C. A. Achete, A. Jorio, and J.-P. Raskin, Nano Research **6**, 269 (2013).
[19]R. W. Havener, H. Zhuang, L. Brown, R. G. Hennig, and J. Park, Nano Lett. **12**, 3162 (2012).
[20]K. Kim, S. Coh, L. Z. Tan, W. Regan, J. M. Yuk, E. Chatterjee, M. F. Crommie, M. L. Cohen, S. G. Louie, and A. Zettl, Phys. Rev. Lett. **108**, 246103 (2012).
[21]K. Sato, R. Saito, C. Cong, T. Yu, and M. S. Dresselhaus, Phys. Rev. B **86**, 125414 (2012).
[22]M. M. Lucchese, F. Stavale, E. H. Ferriera, C. Vilane, M. V. O. Moutinho, R. B. Capaz, C. A. Achete, and A. Jorio, Carbon **48**, 1592 (2010).
[23]E. H. Martins Ferreira, M. V. O. Moutinho, F. Stavale, M. M. Lucchese, R. B. Capaz, C. A. Achete, and A. Jorio, Phys. Rev. B **82**, 125429 (2010).
[24]L. G. Cançado, K. Takai, T. Enoki, M. Endo, Y. A. Kim, H. Mizusaki, A. Jorio, L. N. Coelho, R. Magalhes-Paniago, and M. A. Pimenta, Appl. Phys. Lett. **88**, 163106 (2006).
[25]L. G. Cançado, A. Jorio, E. H. Martins Ferreira, F. Stavale, C. A. Achete, R. B. Capaz, M. V. O. Moutinho, A. Lombardo, T. S. Kulmala, and A. C. Ferrari, Nano Lett. **11**, 3190 (2011).
[26]W.-T. Pong and C. Durkan, J. Phys. D: Appl. Phys. **38**, R329 (2005).
[27]J. T. Robinson, S. W. C. Schmucker, B. Diaconescu, J. P. Long, J. C. Culbertson, T. Ohta, A. L. Friedman, and T. E. Beechem, ACS Nano **7**, 637 (2013).
[28]J. Campos-Delgado, G. Algara-Siller, C. N. Santos, U. Kaiser, and J.-P. Raskin, Small (2013), doi:10.1002/smll.201300050.
[29]A. T. N'Diaye, J. Coraux, T. N. Plasa, C. Busse, and T. Michely, New J. Phys. **10**, 043033 (2008).
[30]P. Poncharal, A. Ayari, T Michel, and J. L. Sauvajol, Phys. Rev. B **78**, 113407 (2008).
[31]Y. Wang, Z. Su, W. Wu, S. Nie, N. Xie, H. Gong, Y. Guo, J. H. Lee, X. Xing, S. Lu, H. Wang, X. Lu, K. McCarty, F. Pei, S. Robles-Hernandez, V. G. Hadjiev, and J. Bao, arXiv:1301.4488 .
[32]C. M. Almeida, V. Carozo, R. Prioli, and C. A. Achete, J. Appl. Phys. **110**, 086101 (2011).
[33]T. Ohta, J. T. Robinson, P. J. Feibelman, A. Bostwick, E. Rotenberg, and T. E. Beechem, Phys. Rev. Lett. **109**, 186807 (2012).
[34]I. Brihuega, P. Mallet, H. Gonzalez-Herrero, G. Trambly de Laissardiere, M. M. Ugeda, L. Magaud, J. M. Gomez-Rodriguez, F. Yndurain, and J.-Y. Veuillen, Phys. Rev. Lett. **109**, 196802 (2012).
[35]J. M. Soler, E. Artacho, J. D. Gale, J. Garcia, A. Junquera, P. Ordejn, and D. Sánchez-Portal, J. Phys.: Condens. Matter **14**, 2745 (2002).
[36]M. A. Pimenta, G. Dresselhaus, M. S. Dresselhaus, L. G. Cançado, A. Jorio, and R. Saito, Phys. Chem. Chem. Phys. **09**, 1276 (2007).
[37]A. M. A. Eckmann, A. Felten, R. Britnell, L. Krupke, K. S. Novoselov, and C. Casiraghi, Nano Lett. **12**, 3925 (2012).
[38]C. Casiraghi, S. Pisana, K. S. Novoselov, A. K. Geim, and A. C. Ferrari, Appl. Phys. Lett. **91**, 233108 (2007).
[39]A. Das, S. Pisana, B. Chakraborty, S. Piscanec, S. K. Saha, U. V. Waghmare, H. R. Novoselov, K. S. Krishnamurthy, A. K. Geim, A. C. Ferrari, and A. K. Sood, Nat. Nanotech. **3**, 210 (2008).
[40]M. C. Prado, R. Nascimento, L. G. Moura, M. J. S. Matos, M. S. C. Mazzoni, L. G. Cançado, H. Chacham, and B. R. A. Neves, ACS Nano **5**, 394 (2010).
[41]M. S. Dresselhaus and G. Dresselhaus, Adv. Phys. **30**, 139 (1981).
[42]W. J. Zhao, P. H. Tan, K. Liu, and A. C. Ferrari, J. Am. Chem. Soc. **133**, 5941 (2011).
[43]D. L. Miller, K. D. Kubista, G. M. Rutter, M. Ruan, W. A. de Heer, P. N. First, and J. A. Stroscio, Phys. Rev. B **81**, 125427 (2010).
[44]T. M. G. Mohiuddin, A. Lombardo, R. R. Nair, A. Bonetti, G. Savini, R. Jalil, N. Bonini, D. M. Basko, C. Galiotis, N. Marzari, K. S. Novoselov, A. K. Geim, and A. C. Ferrari, Phys. Rev. B **79**, 205433 (2009).
[45]A. G. Souza Filho, A. Jorio, G. Dresselhaus, M. S. Dresselhaus, R. Saito, A. K. Swan, M. S. Ünlü, B. B. Goldberg, J. H. Hafner, C. M. Lieber, and M. A. Pimenta, Phys. Rev. B **65**, 035404 (2001).